Inorganic Chemistry
Article
pubs.acs.org/IC

Synthesis, Detailed Characterization, and Theoretical Understanding of Mononuclear Chromium(III)-Containing Polyoxotungstates $[Cr^{III}(HX^{V}W_7O_{28})_2]^{13-}$ (X = P, As) with Exceptionally Large Magnetic Anisotropy

Wenjing Liu,[†] Jonathan H. Christian,[‡,§] Rami Al-Oweini,[†] Bassem S. Bassil,[†] Johan van Tol,[§] Mihail Atanasov,*[,∥,⊥] Frank Neese,*[,∥] Naresh S. Dalal,*[,‡,§] and Ulrich Kortz*[,†]

[†]Jacobs University, School of Engineering and Science, P.O. Box 750561, 28725 Bremen, Germany

[‡]Department of Chemistry and Biochemistry, Florida State University, 95 Chieftan Way, Tallahassee, Florida 32306, United States

[§]National High Magnetic Field Laboratory, Florida State University, 1800 E Paul Dirac Drive, Tallahassee, Florida 32306, United States

[∥]Max-Planck Institute for Chemical Energy Conversion, Stiftstrasse 34-36, 45470 Mülheim/Ruhr, Germany

[⊥]Institute for General and Inorganic Chemistry, Bulgarian Academy of Sciences, 1113 Sofia, Bulgaria

S *Supporting Information*

ABSTRACT: Two monochromium(III)-containing heteropolytungstates, $[Cr^{III}(HP^{V}W_7O_{28})_2]^{13-}$ (**1a**) and $[Cr^{III}(HAs^{V}W_7O_{28})_2]^{13-}$ (**2a**), were prepared via simple, one-pot reactions in aqueous, basic medium, by reaction of the composing elements, and then isolated as hydrated sodium salts, $Na_{13}[Cr^{III}(HP^{V}W_7O_{28})_2]\cdot 47H_2O$ (**1**) and $Na_{13}[Cr^{III}(HAs^{V}W_7O_{28})_2]\cdot 52H_2O$ (**2**). Polyanions **1a** and **2a** comprise an octahedrally coordinated Cr^{III} ion, sandwiched by two $\{PW_7\}$ or $\{AsW_7\}$ units. Both compounds **1** and **2** were fully characterized in the solid state by single-crystal XRD, IR spectroscopy, thermogravimetric and elemental analyses, magnetic susceptibility, and EPR measurements. Magnetic studies on **1** and **2** demonstrated that both compounds exhibit appreciable deviation from typical paramagnetic behavior, and have a ground state $S = {}^{3}/_{2}$, as expected for a Cr^{III} ion, but with an exceptionally large zero-field uniaxial anisotropy parameter (D). EPR measurements on powder and single-crystal samples of **1** and **2** using 9.5, 34.5, and 239.2 GHz frequencies and over 4−295 K temperature fully support the magnetization results and show that $D = +2.4\ cm^{-1}$, the largest and sign-assigned D-value so far reported for an octahedral Cr^{III}-containing, molecular compound. Ligand field analysis of results from CASSCF and NEVPT2-correlated electronic structure calculations on $Cr(OH)_6^{3-}$ model complexes allowed to unravel the crucial role of the second coordination sphere of Cr^{III} for the unusually large magnetic anisotropy reflected by the experimental value of D. The newly developed theoretical modeling, combined with the synthetic procedure for producing such unusual magnetic molecules in a well-defined and essentially magnetically isolated environment, appears to be a versatile new research area.

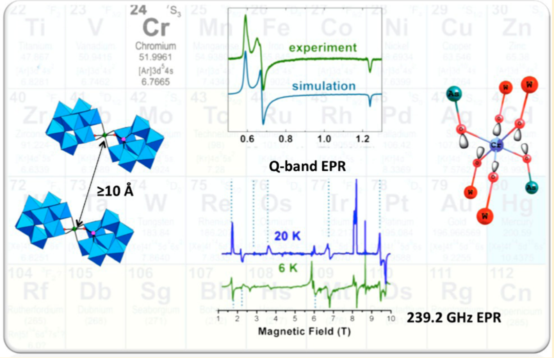

■ INTRODUCTION

The study of polyoxometalates (POMs) in molecular magnetism is an attractive research area because magnetic materials show prospects in integrated information storage, quantum computing devices, biochemistry, and molecule-based magnets.[1] Reactions of lacunary POMs with different magnetic centers such as transition metals, lanthanides, mixed 3d−4f clusters, or polynuclear transition metal clusters have resulted in a plethora of structures with variable magnetic behaviors.[2] In the domain of transition metal-containing POM chemistry, the magnetic properties of POMs incorporating paramagnetic 3d metals such as manganese, iron, cobalt, nickel, and copper have been widely studied.[3] In comparison, chromium-containing POMs are far less explored, mainly due to the kinetic inertness of hexa-aqua Cr^{III} ions toward ligand exchange in solution.[4]

However, the challenge of preparing new Cr-containing POMs remains a highly rewarding research area, since the paramagnetic nature of Cr^{III} can provide a platform for studying magnetic properties at atomic or molecular levels. Many of the earlier EPR studies have been on complexes where Cr^{III} is used as a dopant ion in lattices such as ruby, CaO, and $MgWO_4$, or for probing phase transitions in ferroelectric lattices.[5] Another area of high current interest is developing Cr^{III} complexes with large magnetic anisotropy which can serve as building blocks

Received: June 12, 2014
Published: August 19, 2014

for novel molecular magnets with applications in high-density information storage, quantum computing, and spintronics.[6] Long and co-workers[7a] have made significant progress in this regard, showing that adding ligands with large spin−orbit coupling to Cr^{III} ions and causing large structural distortion to their octahedral coordination could lead to large *D*, as much as 2.3 cm^{-1}. Goswami and Misra[7b] have carried out theoretical analyses in support of this approach, emphasizing that the experimental determination of the sign of the *D* value is an important parameter in understanding the electronic structure of such molecules. Therefore, precise information on the spin state and the magnetic parameters, including their signs, is of fundamental theoretical importance; this factor provided an impetus for the present work.

The number of compounds resulting from interaction of lacunary POMs with paramagnetic Cr^{III} ions is rather small.[8] Wassermann et al. reported the initial result as $[Cr_3(OH)_3(H_2O)_3\text{-}A\text{-}\alpha\text{-}SiW_9O_{34}]^{4-}$, where three Cr^{III} centers are bridged by three hydroxo groups which are fixed on the trivacant tungsten sites in $[A\text{-}\alpha\text{-}SiW_9O_{34}]^{9-}$.[8a] Further condensation of this compound in aqueous solution led to a sandwich-type dimer containing three paramagnetic Cr^{III} ions, $[\{Cr_3(OH)_3SiW_9O_{34}\}_2(OH)_3]^{10-}$.[8b] Subsequently, the dinuclear polyanion $[Cr_2(OH)(OOCCH_3)_2(H_2O)_2SiW_{10}O_{36}]^{5-}$ was reported, in which the two Cr^{III} centers are bridged by two acetato and a hydroxo group.[8c] The trichromium-containing polyanion $[\{Cr(OH)(H_2O)\}_3(SiW_{10}O_{36})_2]^{10-}$ with a $\{Cr_3\}$ core has also been described.[8d] Besides tungsten-based Cr^{III}-containing POMs, two Cr^{III}-substituted sandwich-type polyoxomolybdates, $[Cr_2(AsMo_7O_{27})_2]^{12-}$ and $[CrFe(AsMo_7O_{27})_2]^{12-}$, were also reported.[8e,f] To the best of our knowledge, these are the only reported examples of POM-based Cr^{III} complexes, where the Werner-type chromium-oxo core is usually stabilized by hydroxo or acetato bridging ligands.

Herein, we report on the synthesis and structure of the first two examples of monochromium-containing heteropolytungstates, their magnetic characterization by susceptibility measurements and electron paramagnetic resonance (EPR), as well as state-of-the-art quantum chemistry and efficient implementation of multi reference *ab initio* methods.[9]

EXPERMENTAL SECTION

Synthesis. All chemical reagents were commercially available and used without further purification.

$Na_{13}[Cr^{III}(HP^{V}W_7O_{28})_2]\cdot 47H_2O$ (1). A sample of $Cr(NO_3)_3\cdot 9H_2O$ (0.10 g, 0.25 mmol) was first dissolved in 20 mL of sodium acetate solution (1 M, pH 6) followed by addition of 85% H_3PO_4 (53 μL, 0.8 mmol) and $Na_2WO_4\cdot 2H_2O$ (1.65 g, 5.0 mmol). The mixture was then stirred for 1 h at 80 °C. After the mixture was cooled to room temperature and filtered, the obtained pH was 8. Slow evaporation of the green solution at room temperature led to the formation of green crystals of **1** within 3 days (yield 0.12 g, 10% based on Cr). IR (cm^{-1}): 1071 (s), 1010 (m), 942 (s), 911 (w), 892 (w), 684 (s, br) 519 (m), 439 (w). Anal. Calcd (Found): Na 6.3 (6.5), Cr 1.1 (1.1), P 1.3 (1.4), W 54.4 (53.6). *M* = 4731.46 g/mol.

$Na_{13}[Cr^{III}(HAs^{V}W_7O_{28})_2]\cdot 52H_2O$ (2). A sample of $Cr(NO_3)_3\cdot 9H_2O$ (0.10 g, 0.25 mmol) was first dissolved in 20 mL of sodium acetate solution (1 M, pH 6) followed by the addition of As_2O_5 (0.08 g, 0.36 mmol) and $Na_2WO_4\cdot 2H_2O$ (1.65 g, 5 mmol). The mixture was then stirred for 1 h at 80 °C. After the mixture was cooled to room temperature and filtered, the obtained pH was 8. Slow evaporation of the green solution at room temperature led to the formation of green crystals of **2** after 1 week (yield 0.18 g, 15% based on Cr). IR (cm^{-1}): 1637 (s), 945 (m), 850 (s, br), 679 (s), 519 (m), 427 (w). Anal. Calcd (Found): Na 6.1 (6.3), Cr 1.1 (1.3), As 3.1 (3.2), W 52.4 (51.6). *M* = 4908.50 g/mol.

Instrumentation. Infrared spectra (Supporting Information Figure S1) were recorded on a Nicolet Avatar 370 FT-IR spectrophotometer using KBr pellets. The following abbreviations were used to assign the peak intensities: w = weak; m = medium; s = strong; br = broad. Thermogravimetric analyses were carried out on a TA Instruments SDT Q600 thermobalance with a 100 mL/min flow of nitrogen; the temperature was ramped from 20 to 800 °C at a rate of 5 °C/min. Elemental analyses were performed by CNRS, Service Central d'Analyze, Solaize, France. Temperature-dependent magnetic susceptibility measurements were made using a Quantum Design MPMS-XL-5 SQUID magnetometer over a temperature range 300−1.8 K at a measuring field of 0.01 T. Magnetization measurements at variable temperature and variable field (VTVH) were performed at 1, 3, and 5 T over the temperature range 300−1.8 K. Electron paramagnetic resonance (EPR) spectra were recorded on a Bruker E500 spectrometer equipped with X- and Q-band microwave sources (9.5 and 34.5 GHz, respectively). The frequency was recorded with a built-in digital frequency counter. Variable temperature (4−295 K) high-frequency EPR measurements (239.2 GHz) were conducted at the Florida State University National High Magnetic Field Laboratory (FSU-NHMFL) in Tallahassee, FL. The HF-EPR operates in transmission mode and employs cylindrical waveguides, as described elsewhere.[10] The magnetic field was calibrated using a DPPH standard ($g = 2.0036$).

X-ray Crystallography. Single crystals of **1** and **2** were mounted on a Hampton cryoloop in light oil for data collection at 100 K. Indexing and data collection were measured on a Bruker D8 SMART APEX II CCD diffractometer with kappa geometry [graphite monochromator, λ(Mo Kα) = 0.710 73 Å]. Data integration was performed using *SAINT*.[11] Routine Lorentz and polarization corrections were applied. Multiscan absorption corrections were performed using *SADABS*.[12] Direct methods (*SHELXS*) successfully located the tungsten atoms, and successive Fourier syntheses (*SHELXL*) revealed the remaining atoms.[12] Refinements were full-matrix least-squares against $|F|^2$ using all data. In the final refinement, the Cr, W, P, As, and Na atoms were refined anisotropically, whereas the O atoms were refined isotropically. The complete X-ray crystallographic data for **1** and **2** (CIF format) is available free of charge via the Internet at the FIZ Karlsruhe-Leibniz-Institute http://www.fiz-karlsruhe.de/icsd.html with CSD numbers 427383 and 427384.

Computations and Ligand Field Analysis. DFT and *ab initio* calculations using the entire molecules of the POMs reported here were prohibited due to their large size. Accordingly, we have carried out correlated *ab initio* calculations on $Cr(OH)_6^{3-}$ model complexes. Complete active space self-consistent field (CASSCF) wave functions[13] were employed to account for dynamical correlation via N-electron valence second order perturbation theory (NEVPT2).[14] Basis functions of triple-ζ quality (def2-TZVP)[15] along with corresponding auxiliary functions for numerical calculations were used in all calculations. A DFT geometry optimization with the BP86 functional[16] and the same basis sets yielded DFT optimized geometry of $Cr(OH)_6^{3-}$ for comparison with geometries constrained by next nearest neighbors of Cr^{III}. To analyze the effect of the second coordination sphere on the electronic levels and zero-field splitting of Cr^{III}, CASSCF wave functions as well as both CASSCF and NEVPT2 energy eigenvalues were analyzed employing a mapping procedure[17] yielding ligand field and O−Cr bonding parameters within the angular overlap model.[18] All computations were done with the *ab initio* and DFT computer program ORCA.[9]

RESULTS AND DISCUSSION

Synthesis and Structure. The novel polyanions $[Cr^{III}(HP^{V}W_7O_{28})_2]^{13-}$ (**1a**) and $[Cr^{III}(HAs^{V}W_7O_{28})_2]^{13-}$ (**2a**) were synthesized by interaction of the respective heterogroup (H_3PO_4/As_2O_5) with $Cr(NO_3)_3\cdot 9H_2O$ and $Na_2WO_4\cdot 2H_2O$ in aqueous NaOAc solution (pH 8) at 80 °C.

Polyanions **1a** and **2a** comprise an octahedrally coordinated Cr^{III} ion, sandwiched by two $\{PW_7\}$ or $\{AsW_7\}$ units. The successful synthesis of **1a** and **2a** requires several key reaction conditions, such as the final pH value, which is crucial and should be carefully adjusted to 7.5−8.5, starting with a pH 6 solution. With a pH < 7.5, the desired product could not be isolated, whereas pH > 8.5 resulted in the formation of a precipitate. The formation of **1a** and **2a** also depends on the reaction temperature, which should be in the range 75−95 °C, as lower heating did not lead to the desired products. The choice of solvent is also important, as reaction in plain water under otherwise identical conditions did not provide the title compounds. With respect to the cations present, the corresponding potassium acetate solution resulted in **1** and **2** (as verified by IR and XRD analyses), but with lower yield.

Crystallographic structural analysis revealed that **1** and **2** are isomorphous, both crystallizing in the triclinic space group $P\bar{1}$ (see Table 1). The polyanionic entities $[Cr^{III}(HX^{V}W_7O_{28})_2]^{13-}$ (X = P, **1a**; As, **2a**) consist of two equivalent heptatungstate moieties $[HXW_7O_{28}]^{8-}$, which are arranged almost orthogonally to each other and linked via a single Cr^{III} ion through four "planar" Cr−O−W and two "axial" Cr−O−X bridges. Each moiety consists of a $\{W_3O_{13}\}$ triad linked to an edge-shared half-ring $\{W_4O_{19}\}$ via corner-sharing, with both units stabilized by the central $\{XO_4\}$ group. This structure results therefore in a C_{2h} point-group symmetry, with the C_2 axis passing through the Cr^{III} center (Figure 1). The heptatungstate fragment has been reported before by our group in the ruthenium-containing $[Ru(dmso)_3HPW_7O_{28}]^{6-}$, which was also studied in solution via multinuclear NMR.[19] Recently, similar transition metal-sandwiched compounds with the same structure $[M(HPW_7O_{28})_2]^{n-}$ (n = 13, M = Fe^{III}, Mn^{III}; n = 14, M = Co^{II}, Cd^{II}, Mn^{II}), were also reported.[20]

Table 1. Crystal Data for $Na_{13}[Cr^{III}(HP^{V}W_7O_{28})_2]\cdot 47H_2O$ (1) and $Na_{13}[Cr^{III}(HAs^{V}W_7O_{28})_2]\cdot 52H_2O$ (2)

	1	2
formula	$Na_{13}[Cr(HPW_7O_{28})_2]\cdot 47H_2O$	$Na_{13}[Cr(HAsW_7O_{28})_2]\cdot 52H_2O$
fw, g/mol	4731.47	4909.45
cryst syst	triclinic	triclinic
space group	$P\bar{1}$	$P\bar{1}$
a, Å	10.4928(3)	10.5336(8)
b, Å	10.9461(3)	10.9707(9)
c, Å	20.8919(6)	21.0169(18)
α, deg	85.1820(10)	85.119(5)
β, deg	77.2760(10)	77.571(4)
γ, deg	67.3550(10)	67.134(4)
V, Å^3	2160.17(11)	2185.4(3)
Z	1	1
D_{calcd}, g/cm^3	3.637	3.730
$F(000)$	2153	2239
cryst size, mm^3	0.2 × 0.15 × 0.02	0.15 × 0.12 × 0.02
R(int)	0.0522	0.0721
obsd ($I > 2\sigma(I)$)	7566	10 929
GOF on F^2	1.004	1.011
R1 $[I > 2\sigma(I)]^a$	0.0256	0.0308
wR2 (all data)^b	0.0665	0.0772

$^aR = \Sigma||F_o| - |F_c||/\Sigma|F_o|$. $^bR_w = [\Sigma w(F_o^2 - F_c^2)^2/\Sigma w(F_o^2)^2]^{1/2}$.

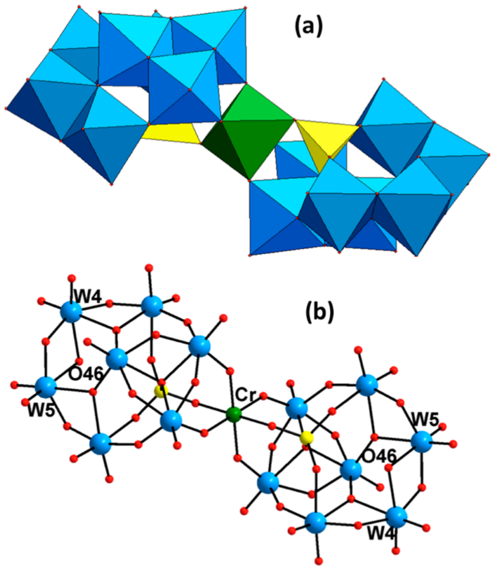

Figure 1. Polyhedral (a) and ball-and-stick (b) representations of polyanions **1a** and **2a**. Color code: X = P, As (yellow), W (blue), Cr (green), O (red).

The highly vacant heptametalate subunits are few in POM literature. To the best of our knowledge, only five types of heptatungstate $\{XW_7\}$ (X = P^{V},[19,20] As^{V},[19] V^{V},[21] Te^{IV},[22] Co^{II} [23]) and two types of heptamolybdate $\{XMo_7\}$ (X = As^{V},[8e,f,24] Fe^{III} [25]) subunits are known (Supporting Information Table S1). The $\{PW_7\}$ building block is structurally similar to the $\{AsW_7\}$ and $\{VW_7\}$ fragments; however, it is different from $\{TeW_7\}$ (Supporting Information Figure S2b) and $\{CoW_7\}$ (Supporting Information Figure S2c) found in $[Te_2W_{16}O_{58}(OH)_2]^{14-}$, $[Te_2W_{18}O_{62}(OH)_2]^{10-}$, and $[Co_7(H_2O)_2(OH)_2P_2W_{25}O_{94}]^{16-}$.[22,23] The $[TeW_7O_{28}]^{10-}$ fragment can be obtained from the trivacant Keggin $[\beta\text{-}TeW_9O_{33}]^{8-}$, by the loss of two WO_6 octehedra, whereas $\{HCoW_7O_{28}\}$ consists of seven edge-shared WO_6 octahedra stabilized by a central CoO_4 tetrahedron.[23] The structures of $\{AsMo_7\}$ and $\{FeMo_7\}$ are very similar to $\{CoW_7\}$, and both can be obtained from the trivacant Keggin ion $\{XM_9O_{33}\}$ by loss of one $\{M_3O_{13}\}$ triad and insertion of one MO_6 octahedron into the cavity between the two triad units.

The central Cr^{III} ion adopts a distorted octahedral geometry with three different types of μ-oxo bridges: two from four $\{WO_6\}$ octahedra of the $\{W_3O_{13}\}$ triads (**1**, Cr−O, 1.953(5)−1.956(5) Å; **2**, Cr−O, 1.953(5)−1.975(5) Å) and one from the hetero group XO_4 (**1**, Cr−O, 1.996(5) Å; **2**, Cr−O, 1.999(5) Å). In comparison, the Fe−O bond lengths in $[Fe^{III}(HPW_7O_{28})_2]^{13-}$ are relatively longer (1.984(6)−2.039(7) Å), in full agreement with the size difference between Cr^{III} (r = 0.615 Å) and Fe^{III} (r = 0.645 Å)..[8f,20b] For the $\{HPW_7O_{28}\}$ subunit, four kinds of W−O bond lengths fall within the anticipated ranges for the different types of oxo ligands with an increasing trend: terminal (1.713(5)−1.746(5) Å), μ_2-bridging (1.883(5)−1.958(5) Å), μ_3-bridging (1.900(5)−2.300(5) Å), and μ_4-bridging (2.335(4)−2.357(4) Å). Moreover, one of four oxygen atoms of the PO_4 tetrahedron in $[HPW_7O_{28}]^{8-}$ connects to one Cr^{III} ion, leading to its distortion. The three P-μ_2-O bond lengths differ slightly (1.515(5)−1.531(5) Å), while the P-μ_4-O (the central O of the triad) is expectedly longer (1.580(5) Å). In the case of $\{HAsW_7O_{28}\}$, the As−O bond lengths are in the range 1.667(5)−1.721(4) Å. Selected bond lengths and angles for **1** and **2** are shown in Supporting Information Table S2.

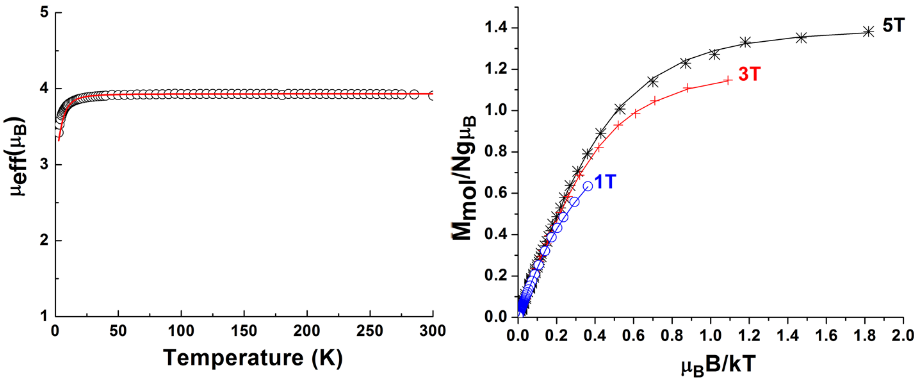

Figure 2. (a) μ_{eff} versus T of compound **2**. (b) VTVH magnetization measurements of **2** at 1, 3, and 5 T. The solid lines represent the best fits to the experimental data.

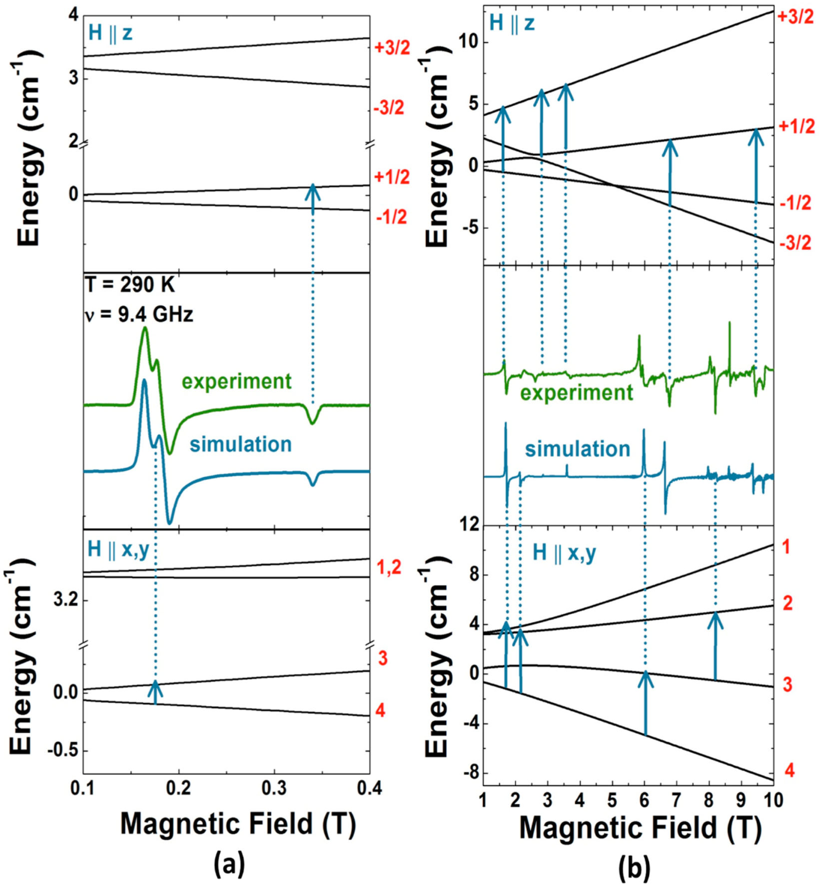

Figure 3. (a) X-band (9.4 GHz) EPR experimental computer simulated spectra of **2**. The top and bottom portions show the energy level diagrams for the $H \| z$ (principal symmetry axis of the molecule) and the perpendicular x, y directions. The red numbers in the top figure represent the M_s quantum numbers in the high-field limit. In the bottom figure, however, they are just a label for an energy level since the field strength was not enough to be in the "high-field" limit. Blue arrows mark the EPR transition assignment. (b) 239.2 GHz EPR experimental and simulated spectra of **2** at 6 K with the energy level diagrams both parallel and perpendicular to the principal symmetry axes (as marked). Blue arrows show the EPR transition assignments. The red numbers are as described above.

In the solid state, the polyanions are surrounded by sodium countercations, which in turn coordinate to crystal water molecules (Supporting Information Figures S3 and S4). X-ray diffraction and elemental analysis confirmed that there are 13 Na^+ ions in total per polyanion. Bond valence sum (BVS) calculations show, for each $\{HPW_7O_{28}\}$ subunit in **1**, that the bridging oxo O46 is monoprotonated with W–O bond lengths of 2.167(5) and 2.183(5) Å and a BVS of 0.91, which is the value expected for a hydroxo group. This gives a total charge of −13 for **1a**, which is stabilized in the solid state by sodium countercations. The same applies for compound **2**, with the hydroxo group located at O37 (Supporting Information Table S3).

Magnetic Studies. Detailed magnetic characterization of **1** and **2** is of high interest because they are rare instances of Cr^{III}, a $3d^3$ ion, in a well-defined geometry with six covalently bonded oxo ligands. Each Cr^{III} ion is surrounded by many diamagnetic atoms which magnetically insulate the Cr ions from each other,

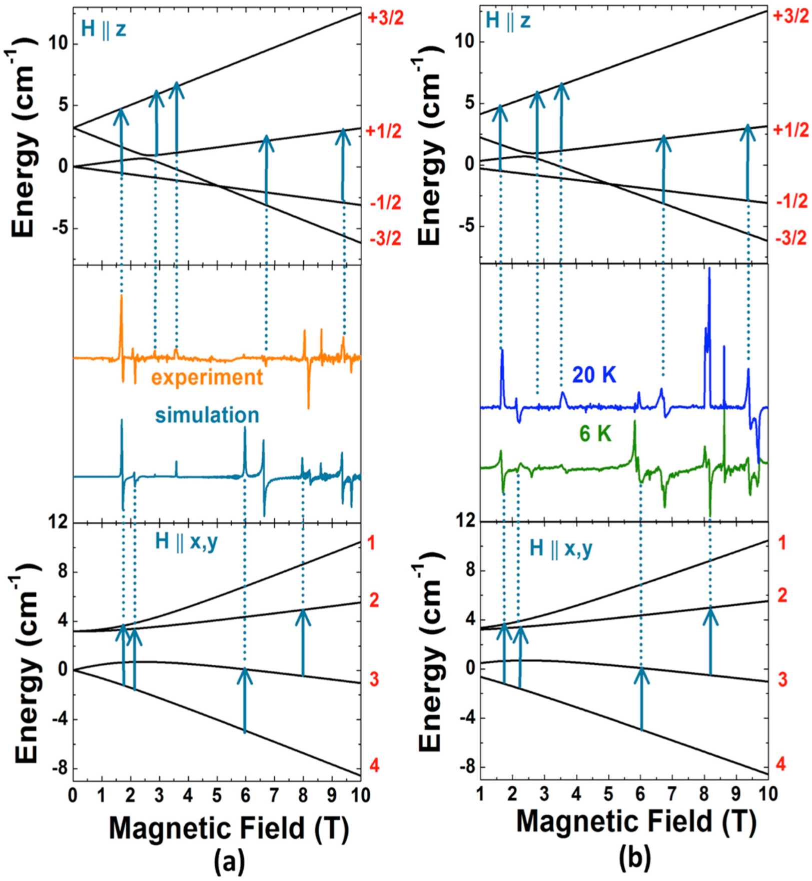

Figure 4. (a) High-frequency (239.2 GHz) EPR experimental and simulation spectra of **1** at 8 K are shown with the energy level diagram for the principal symmetry axis, $H \| z$, and the perpendicular *x*, *y* directions. The blue arrows mark the EPR transition assignments. (b) High-frequency (239.2 GHz) experimental EPR spectra of **2** at 20 and 6 K are shown with the energy level diagram, which was derived from the best simulation of these spectra. The sign of *D* was determined by comparison of the relative line intensities in the two spectra. Upon cooling from 20 to 6 K the transitions at ∼6 and ∼6.8 T, which correspond to the lowest lying energy states, become more intense, while the transitions at ∼8.2 and 3.6 T, which correspond to the highest energy transitions, become less intense. The results are in excellent agreement with the Boltzmann distribution.

the nearest neighbor $\mathrm{Cr^{III}}$ ion distance being ≈10 Å. This situation is particularly suitable for characterization by EPR, since the lack of dipolar couplings with the nearest neighbors should lead to narrow EPR peaks and thus higher precision for the measurement of magnetic parameters. Distorted octahedral $\mathrm{Cr^{III}}$ complexes usually show small zero-field splitting since the ground states and excited states are generally well-separated. As shown below, however, the zero-field parameters of **1** and **2** are found to be unexpectedly large.

As a start, magnetic susceptibility (χ) measurements were undertaken to establish the electronic spin of the $3d^3$ configuration, which is expected to be $S = {}^3/_2$, a spin-quartet. Figure 2 shows the measured temperature dependence of the magnetic moment, μ_{eff}, of **2** from 1.8 to 300 K. The magnetic moment is 3.90 μ_B at room temperature, which is close to the spin-only value for $S = {}^3/_2$ (3.87 for $g = 2$). This value remains nearly constant at high temperature, but sharply decreases to 3.3 μ_B below 20 K. Due to the significant Cr−Cr distance in both compounds it was hypothesized that this decrease was due to magnetic interactions within each molecule (spin−spin and spin−orbit coupling) rather than intermolecular *J* coupling. Such interactions result in zero-field splitting of the electronic eigenstates. Therefore, the magnetic properties of both compounds were evaluated using the following standard spin Hamiltonian of a system with $S = {}^3/_2$.

$$\hat{H} = \beta \mathbf{H}\cdot\mathbf{g}\cdot\hat{\mathbf{S}} + D(\hat{S}_z^{\,2} - \hat{\mathbf{S}}^2/3) + E(\hat{S}_x^{\,2} - \hat{S}_y^{\,2}) \qquad (1)$$

In this Hamiltonian, **g** is the Zeeman tensor, *D* and *E* are the axial and rhombic second order zero-field splitting parameters, and the other terms pertain their usual meaning.[26] The hyperfine interaction is omitted because the magnetic isotope of Cr (i.e., ^{53}Cr, with $I = {}^3/_2$) has rather small (∼9.5%) natural abundance; thus, each peak of the hyperfine quartet would be ∼2.5% of the main peaks. The temperature dependence of the magnetic susceptibility is derived from diagonalization of the Hamiltonian matrix.[27,28] The data in Figure 2 yielded an acceptable fit using the following parameters: $S = {}^3/_2$, $g = 2.02$, and $D = 3.6\ \mathrm{cm^{-1}}$, and a small $E/D = 0.04$. These data indicate that *D* is exceptionally large, since the literature values of $\mathrm{Cr^{III}}$ complexes range from 0.107 to 1.28 $\mathrm{cm^{-1}}$,[5,29,7a] with the sole exception of $D = 2.3\ \mathrm{cm^{-1}}$ found for the octahedral complex $[\mathrm{Cr(dmpe)_2(CN)I}]$ [dmpe = 1,2-bis(dimethylphosphino)-ethane],[7] although no EPR is provided for the afformentioned compound and the results herein are thus considered a significant addition to this field. Fitting of variable temperature/variable field (VTVH) magnetization measurements of **2** (Figure 2, right) yields similar magnetic parameters of $g = 2.03$ and a slightly lower *D* (2.5 $\mathrm{cm^{-1}}$). Similar measurements on **1** are shown in Supporting Information Figure S7 and were well fit to the same parameters as **2** except with $E/D = 0.02$.

Since χ is not an accurate method for determining D or g, a detailed EPR study was undertaken.

EPR Measurements. Figure 3a shows the room temperature, X-band (9.4 GHz) powder EPR spectrum of **2** (middle segment, green trace). Also shown are the simulated energy level diagrams, obtained using a locally developed computer program, for H along the principal symmetry axis of the molecule ($H \| z$) and along the perpendicular x, y directions (top and bottom segment respectively). Two distinct g-tensor components are seen at $g_{\|}' = 1.975$ and $g_{\perp}' = 3.752$. Such large anisotropy is evidence of significant zero-field splitting; thus, the g values are labeled with prime symbols indicating they are effective values. For $S = {}^3/_2$ with a large D (i.e., $D \gg$ microwave quantum), the effective and real g values are related by $g_{\perp} = g_{\perp}'/2$ and $g_{\|} = g_{\|}'$.[30] Therefore, the actual g values are $g_{\|} = 1.975$ and $g_{\perp} = 1.876$. There is slight splitting in the perpendicular line due to small anisotropy between the x and y directions. This feature is not seen in **1**, likely due to even smaller rhombic distortion (Supporting Information Figure S8). At Q-band frequency (34 GHz), both materials show clear splitting in the perpendicular peaks (Supporting Information Figure S9), suggesting the need for high field EPR (HF-EPR).

Furthermore, the absence of 9 peaks expected for a $S = {}^3/_2$ ion in a distorted octahedral geometry also suggested that the D-value must be much larger than the Q-band microwave quantum (1.1 cm^{-1}).[31] Computer simulated spectra (middle segment, blue trace), obtained using a locally developed program[10,32] were in good agreement with the experimental data, and yielded the following: $S = {}^3/_2$, g_z =1.97−2.00, $g_{x,y}$ = 1.92−1.94, $|D|$ = 2.4−2.8 cm^{-1}, and E/D = 0.02−0.04.

Since D and E are related to $g_{\|}$ (g_z) and $g_{\perp}$ (g_x, g_y) via[31]

$$D(^4T_2) = \frac{\zeta_{Cr}}{6}\left[g_{zz} - \frac{1}{2}(g_{xx} + g_{yy})\right]$$

$$E(^4T_2) = \frac{\zeta_{Cr}}{12}(g_{xx} - g_{yy}) \qquad (2)$$

where ζ_{Cr} is the spin−orbit coupling constant, ∼ 210 cm^{-1} for Cr^{III},[29e] D and E must be large and positive, which is a surprising result when compared with the literature data. Since interstitial water solvent might easily have been lost from the powder sample, the powder data were confirmed through single-crystal angular dependence Q-band EPR (Supporting Information Figure S10). In order to obtain precise values for these parameters, we undertook EPR measurements using frequencies higher than 3 cm^{-1}, i.e., initiated high-frequency EPR (HF-EPR).

Figure 3b shows the 239.2 GHz experimental spectrum of **2** (middle segment, green trace) and the simulated spectra (middle segment, blue trace). Simulations were performed using the same program and parameters as in Figure 3a. Although the spectrum becomes increasingly complicated at such high frequencies, it is seen that there is a fine agreement between the experimental and simulated spectra with minor artifacts due to an imperfectly random distribution of crystallites in the powder sample. The top and bottom portions of the figure once again display the energy level diagrams both parallel and perpendicular to the principal symmetry axis, while the blue arrows indicate the observed EPR transitions. The high-frequency experimental spectrum and simulation of **1** are shown in Figure 4a. The sign of D was determined by the comparison of the relative line intensities in the 20 and 6 K spectra of **2** as well as comparison of best-fit simulations for $+D$ and $-D$ parameters (Figures 4b and 5). These results clearly suggest that the magnitude and sign of D and E are D = 2.4 cm^{-1} and E/D = 0.05. They also confirm the above conclusion that the zero-field splitting is significantly higher than any seen for Cr^{III} in the literature.[5,7a,29] Below we present *ab initio* DFT model calculations that enable us to understand this unusual finding.

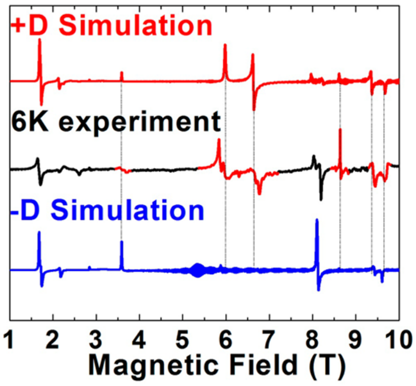

Figure 5. High-frequency (239.2 GHz) experimental EPR spectra of **1** at 6 K (black trace) along with the best fit simulations using positive and negative D (red and blue traces, respectively). The red peaks in the experimental spectrum are drawn to emphasize the key similarities between the $+D$ simulation and the experiment. The dashed lines indicate the fine agreement between the $+D$ simulation with the experiment along with the disagreement between the experiment and $-D$.

Theoretical Analysis of the Origin of the Large *D*. The d^3 configuration of octahedral Cr^{III} spans a $^4A_2(t_2^3)$ ground state and $^4T_2$, $^4T_1^a$, and $^4T_1^b$ excited states. Trigonal distortions (D_3 symmetry) cause a splitting of the states T_2 and T_1 terms into A_1, E and A_2, E sublevels, respectively, and spin−orbit coupling leads to mixing of the trigonally split $^4T_2$ terms bearing first-order angular momenta into the $^4A_2$ ground state spin sublevels. The combined effect of trigonal symmetry and spin−orbit coupling leads to orbital moments into the $^4A_2$ ground state, and this is the cause of the zero-field splitting (2D): the splitting of the $S = {}^3/_2$ spin state into two Kramers doublets with $M_s = \pm{}^3/_2$ and $M_s = \pm{}^1/_2$. Third-order perturbation theory yields eq 3 for D and E with leading contributions from $^4T_2(t^2_e)$ [$^2T_2(t_2^3)$ excited states also contribute to D and E,[33] and they were accounted for in the *ab initio* calculations, but for simplicity will not be considered here]:

$$D(^4T_{2g}) = \frac{4}{9}\zeta_{eff}^2 \frac{E(^4T_2, x0) - E(E(^4T_2, x \pm\ )}{(10Dq)^2}$$

$$E(^4T_{2g}) = \frac{2}{9}\zeta_{eff}^2 \frac{E(^4T_2, x +\ ) - E(^4T_2, x -\ )}{(10Dq)^2} \qquad (3)$$

In eq 3, ζ_{eff} is the effective spin−orbit coupling parameter of Cr^{III} (free ion value 273 cm^{-1}[34]), and 10Dq (typical values for CrO_6^{3-} chromophores 16 000 cm^{-1})[34] and $\Delta E_{trig} = E(^4T_2x\pm) - E(^4T_2, x0)$, respectively, are the cubic ($^4T_2$−$^4A_2$) and trigonal $^4T_{2g}(t_2^2e)$ ligand field splittings. Angular overlap model considerations (eq 4[35]) allow one to relate the trigonal splitting $E(^4T_2, x0) - E(E(^4T_2x\pm\ )$ with the trigonal distortion [$\delta\theta > 0(\delta\theta < 0)$ − trigonal compression (elongation) of the O_h

geometry, θ_{O_h} = 54.735/180] and the Cr—O σ- and π-bonding parameters e_σ and e_π:

$$\Delta E_{\text{trig}} = 3\sqrt{2}(\delta\theta)e_\pi - 18(e_\sigma\delta\theta)^2/10\text{Dq} \tag{4}$$

While the first term on the right-hand site of eq 4 reflects a splitting of the t_2 orbital that depends on the sign of $\delta\theta$, the second one is always negative and tends to stabilize $^4T_2x\pm$ below $^4T_2x0$. If metal—ligand π interactions are not exclusively large (as is usually the case), this second term, according to eq 4, will lead to a positive D. This is the case for the CrO_6 cores discussed here in **1** and **2**. However, with the adoption of a CrO_6 geometry given by the X-ray structures of **1** and **2** (very close to O_h) eqs 3 and 4 yield values of D ($\cong$0.05 cm^{-1}) much smaller than the experimental ones. With influences due to the second coordination sphere of Cr^{III}, the formally highly charged cations W^{VI} and P^V/As^V are expected to largely lower the symmetry. With W^{IV} and As^V/P^V involved in bonds with O that are stronger than the Cr^{III}—O one, a large misalignment of the oxygen lone pairs with respect to the Cr—O bond direction is expected to occur (Figure 6).

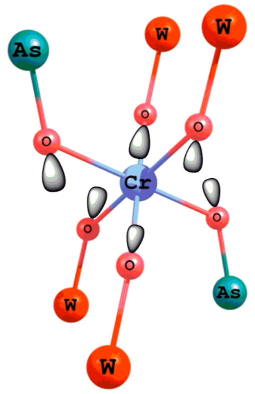

Figure 6. Misdirected valence imposed by the next nearest neighbors of Cr^{III} as possible origin for high D-values. The misalignment of the oxygen lone pairs defined by the angle between the axis of the W—O and As—O bonds and the corresponding Cr—O bond direction (∠AsOCr = 124.4°; ∠WOCr = 141.2, 140.6°) are visualized. The centroids of these lone pairs define an angular distortion toward an extreme trigonal-flattening of the octahedron.

The orientation of these lone pairs is governed by the electron density on the O—W^{VI} and O—$P(As)^V$ bonds in directions opposite to the lone pairs. Such "misdirected valence" was found to alter the donor properties of O, the Cr—O bond, and the ligand field caused by the oxygen ligand resulting in spectacular spectroscopic behavior.[35] Assuming here a hybridization of the oxygen orbitals of sp-type, one observes, e.g., for **2** a larger misalignment of the O lone pairs with respect to the Cr—O bond axis for the Cr—O—As bridge (55.53°) than for the Cr—O—W bridges (angles 38.8° and 39.4°, Figure 6). This results in an effectively compressed geometry and affects the signs and magnitude of the ZFS tensor parameters: the positive value of D and nonvanishing E. Correlated calculations on CrO_6^{3-} model complexes with a variable second coordination sphere of Cr—O (Figure 7) show that O donor functions are indeed strongly modified by the nature and geometry of the atoms or groups attached to O. With a linear Cr—O—H geometry (sp-hybridization, model 1) both σ- and π-oxygen donor character is computed. It induces small trigonal and even a smaller orthorhombic t_2 splitting. A DFT optimized $Cr(OH)_6^{3-}$ complex with an angle Cr—O—H close to 90° represents a basically p^3-type O donor, with a smaller e_σ and a *vanishing* e_π energy. The computed trigonal t_2 splitting is twice larger than in the previous case and correlates with a twice larger D (Table 2). Quite interestingly, switching to a sp O-donor by taking linear Cr—O—H arrangement but not changing the geometry of the CrO_6 leads to a drastic lowering of e_σ and to a nonzero e_π (Table 2). The resulting lowering of 10Dq leads to a narrowing the $^4A_2$—$^4T_2$ gap and to an enhanced mixing of the two states via spin—orbit coupling and trigonal field. Taken together, this leads to an increase of D by a factor of 3 (Table 2). Finally, increasing the formal charge of the atom attached to O from 1 (H, model 1) to 3 ($Cr(OBF)_6^{3+}$ model 3) induces a strong trigonal t_2 splitting and a value of D = 2.255 cm^{-1} which fortuitously matches closely the experimental value reported here (2.4 cm^{-1}). The underlying reason for the experimental result is thus a density deformation due to atoms directly attached to O which violates the apparent geometry of the CrO_6 core (regular close to O_h) in **1** and **2**. An inspection of Figure 6 shows that this deformation is large and in a direction toward a pseudoplanar hexagon.

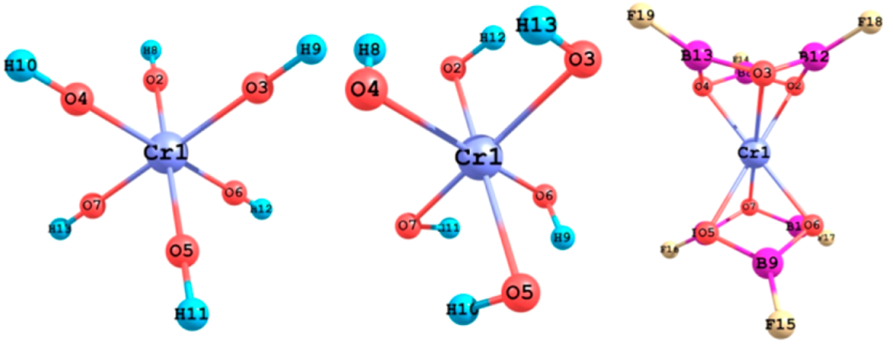

Figure 7. Model complexes for analysis of the correlation between the zero-field splitting D and the Cr—O bonding: model 1(left), $Cr(OH)_6^{3-}$ with linear Cr—O—H bond and a geometry of the CrO_6 core identical with that of the X-ray geometry of **2**; model 2 (middle), a BP86 DFT optimized $Cr(OH)_6^{3-}$ with a bent Cr—O—H geometry due to strong Cr—OH···O intramolecular hydrogen bond (O···H distances 2.089—2.096 Å); model 3 (right), the hypothetical bis(trifluoroboroxine) Cr^{III} complex [$Cr(OBF)_6^{3-}$] with a strongly distorted CrO_6^{3-} core and charge density due to the contrapolarizing B^{3+} attached to O.

Table 2. Characteristic Angles ∠Cr−O−X and ∠O−Cr−O (in deg), Cr−O Angular Overlap Bonding Parameters e_σ and e_π (in cm^{-1}), and t_2 and e Orbitals Energies Due to the Dominating Trigonal and Smaller Orthorhombic Ligand Fields of CrO_6^{3-} from NEVPT2 Calculations[a]

	model 1 $Cr(OH)_6^{3-}$	model 2 $Cr(OH)_6^{3-}$		model 3 $Cr(OBF)_6^{3-}$	$CrO_6W_4As_2$ (**2**)
∠Cr−O−X	180	85.8	180	87.7	124.4 (As); 140.6, 141.2 (W)
∠O−Cr−O	91.0	83.1	83.1	67.3	90.0, 90.2, 92.7
e_σ	5559	4552	3354	6409	
e_π	2086	0	934	0	
D	0.356	0.621	1.87	2.255	2.40
E	0.032	0.005	0.004	0.000	0.12
t_2t_2	0	0	0	0	
t_2	162	273	138	312	
t_2	380	603	930	3526	
e	7917	13 438	6544	16 138	
e	9146	13 811	6724	16 419	

[a] Bonding parameters from ligand field analysis of the *ab initio* results on model complexes, showing dependence on the nature and geometry of the next nearest neighbors of Cr^{III}, angles (in deg) and zero-field splitting parameters *D* and *E* (in cm^{-1}) for the three model compounds. Those for the *trans* $CrO_6W_4As_2$ core in **2** are listed for comparison. See figure for a visualization of model 1, model 2 and model 3.

■ CONCLUSIONS

We have prepared the first examples of mono-Cr^{III}-containing POMs, $[Cr^{III}(HP^VW_7O_{28})_2]^{13-}$ (**1a**) and $[Cr^{III}(HAs^V W_7O_{28})_2]^{13-}$ (**2a**), by reaction of the composing elements in pH 8 sodium acetate medium. Both compounds were fully characterized in the solid state by IR spectroscopy, single-crystal XRD, elemental and thermal analyses, and SQUID and EPR measurements. Polyanions **1a** and **2a** comprise an octahedrally coordinated Cr^{III} ion, sandwiched by two $\{PW_7\}$ or $\{AsW_7\}$ units. Detailed SQUID and EPR spectroscopic measurements on the hydrated sodium salts of **1a** and **2a** showed that the axial zero-field splitting parameter (*D*) is unexpectedly large (2.4 cm^{-1}) for a Cr^{III} ion in an octahedral oxo-coordination. The unusually large value of *D* has been rationalized using *ab initio* calculations and subsequent ligand field analysis. The results show that Cr−O bonding is strongly modified by the polarizing, high-valent ions W^{VI} and As^V. These ions cause misaligned lone pairs and charge density deviating from the X-ray geometry of the CrO_6 core. The large distortion in the axial direction as well as in the equatorial plane of the CrO_6 octahedron reduces the gap between the t_{2g} and the e_g orbitals, and imposes a large trigonal splitting of the metal-centered multiplets. This distortion splits the excited orbital triplet state, and the splitting reacts back through the spin−orbit coupling to remove the degeneracy of the ground spin states. The large distortion along the *z*-axis leads to the large *D*, while the equatorial distortion leads to the nonzero *E*. Similar second-sphere ligand field effects on oxygen ligator ions have been reported in the d−d absorption spectra and EPR of 3d metals in oxidic solids.[35] In addition to this new theoretical insight, we also note the synthetic potential associated with the discovery of **1a** and **2a**. Possibly, the $\{XW_7\}$ fragments present in **1a** and **2a** can be used as building blocks for other POM structures, and such work is currently underway. Also, we have already prepared several other, novel Cr-containing POMs, and this work will be presented elsewhere.

■ ASSOCIATED CONTENT

Ⓢ Supporting Information

X-ray crystallography, supplementary structural figures, IR spectra, other EPR experimental and simulation spectra, TGA curves, and CIF data. This material is available free of charge via the Internet at http://pubs.acs.org.

■ AUTHOR INFORMATION

Corresponding Authors

*E-mail: mihail.atanasov@cec.mpg.de.
*E-mail: Frank.Neese@cec.mpg.de.
*E-mail: dalal@chem.fsu.edu.
*E-mail: u.kortz@jacobs-university.de. Fax: (+49) 421-200-3229. Homepage: www.jacobs-university.de/ses/ukortz.

Notes

The authors declare no competing financial interest.

■ ACKNOWLEDGMENTS

U.K. thanks the German Science Foundation (DFG-KO-2288/20-1) and Jacobs University for research support. W.L. thanks the China Scholarship Council (CSC) for a doctoral fellowship. We also acknowledge the CMST COST Action CM1203 (PoCheMoN) for support. HF-EPR measurements were carried out at the NHMFL, which is supported by National Science Foundation Cooperative Agreement DMR-0654118, the State of Florida, and the U.S. Department of Energy. J.H.C. and N.S.D. thank Catherine Kent and Charles Ingram for valuable assistance with magnetic measurements. Figure 1 was generated by Diamond, Version 3.2 (copyright Crystal Impact GbR).

■ REFERENCES

(1) (a) Christou, G. *Acc. Chem. Res.* **1989**, *22*, 328−335. (b) Pope, M. T.; Müller, A. *Angew. Chem., Int. Ed. Engl.* **1991**, *30*, 34−48. (c) Gatteschi, D.; Pardi, L.; Barra, A. L.; Müller, A.; Döring, J. *Nature* **1991**, *354*, 463−464. (d) Taft, K. L.; Papaefthymiou, G. C.; Lippard, S. J. *Inorg. Chem.* **1994**, *33*, 1510−1520. (e) Clemente-Juan, J. M.; Coronado, E. *Coord. Chem. Rev.* **1999**, *193−195*, 361−394. (f) Müller, A.; Kögerler, P.; Dress, A. W. M. *Coord. Chem. Rev.* **2001**, *222*, 193−218. (g) Poblet, J. M.; Lopez, X.; Bo, C. *Chem. Soc. Rev.* **2003**, *32*, 297−308. (h) Choi, K.-Y.; Matsuda, Y. H.; Nojiri, H.; Kortz, U.; Hussain, F.; Stowe, A. C.; Ramsey, C.; Dalal, N. S. *Phys. Rev. Lett.* **2006**, *96*, 107202. (i) AlDamen, M. A.; Clemente-Juan, J. M.; Coronado, E.; Martí-Gastaldo, C.; Gaita-Ariño, A. *J. Am. Chem. Soc.* **2008**, *130*, 8874−8875. (j) Kortz, U.; Müller, A.; van Slageren, J.; Schnack, J.; Dalal, N. S.; Dressel, M. *Coord. Chem. Rev.* **2009**, *253*, 2315−2327. (k) Ibrahim, M.; Lan, Y.; Bassil, B. S.; Xiang, Y.; Suchopar, A.; Powell, A. K.; Kortz, U. *Angew. Chem., Int. Ed.* **2011**, *50*, 4708−4711. (l) Song, Y. F.; Tsunashima, R. *Chem. Soc. Rev.* **2012**, *41*, 7384−7402. (m) Terazzi, E.; Rogez, G.; Gallani, J.-L.; Donnio, B. *J. Am. Chem. Soc.* **2013**, *135*, 2708−2722. (n) Choi, K. Y.; Wang, Z. X.;

Nojiri, H.; van Tol, J.; Kumar, P.; Lemmens, P.; Bassil, B. S.; Kortz, U.; Dalal, N. S. *Phys. Rev. Lett.* **2012**, *108*, 067206.

(2) (a) Andres, H.; Clemente-Juan, J. M.; Aebersold, M.; Güdel, H. U.; Coronado, E.; Büttner, H.; Kearly, G.; Melero, J.; Burriel, R. *J. Am. Chem. Soc.* **1999**, *121*, 10028−10034. (b) Borrás-Almenar, J. J.; Clemente-Juan, J. M.; Coronado, E.; Tsukerblat, B. S. *Inorg. Chem.* **1999**, *38*, 6081−6088. (c) Kortz, U.; Nellutla, S.; Stowe, A. C.; Dalal, N. S.; Rauwald, U.; Danquah, W.; Ravot, D. *Inorg. Chem.* **2004**, *43*, 2308−2317. (d) Ishikawa, N.; Sugita, M.; Wernsdorfer, W. *Angew. Chem., Int. Ed.* **2005**, *44*, 2931−2935. (e) Mialane, P.; Duboc, C.; Marrot, J.; Rivière, E.; Dolbecq, A.; Sécheresse, F. *Chem.—Eur. J.* **2006**, *12*, 1950−1959. (f) Todea, A. M.; Merca, A.; Bögge, H.; van Slageren, J.; Dressel, M.; Engelhardt, L.; Luban, M.; Glaser, T.; Henry, M.; Müller, A. *Angew. Chem., Int. Ed.* **2007**, *46*, 6106−6110. (g) Tasiopoulos, A. J.; Milligan, P. L.; Abboud, K. A.; O'Brien, T. A.; Christou, G. *Inorg. Chem.* **2007**, *46*, 9678−9691. (h) Zhao, J.-W.; Zhang, J.; Zheng, S.-T.; Yang, G.-Y. *Chem. Commun.* **2008**, 570−572. (i) Sessoli, R.; Powell, A. K. *Coord. Chem. Rev.* **2009**, *253*, 2328−2341. (j) Stamatatos, T. C.; Oliver, K.; Abboud, K. A.; Christou, G. *Inorg. Chem.* **2011**, *50*, 5272−5282. (k) Fang, X.; McCallum, K.; Pratt, H. D., III; Anderson, T. M.; Dennis, K.; Luban, M. *Dalton Trans.* **2012**, *41*, 9867−9870.

(3) (a) Pichon, C.; Mialane, P.; Dolbecq, A.; Marrot, J.; Rivière, E.; Keita, B.; Nadjo, L.; Sécheresse, F. *Inorg. Chem.* **2007**, *46*, 5292−5301. (b) Compain, J.-D.; Mialane, P.; Dolbecq, A.; Mbomekallé, I. M.; Marrot, J.; Sécheresse, F.; Rivière, E.; Rogez, G.; Wernsdorfer, W. *Angew. Chem., Int. Ed.* **2009**, *48*, 3077−3081. (c) Fang, X.; Kögerler, P.; Speldrich, M.; Schilder, H.; Luban, M. *Chem. Commun.* **2012**, *48*, 1218−1220. (d) Zheng, S.-T.; Yang, G.-Y. *Chem. Soc. Rev.* **2012**, *41*, 7623−7646. (e) Al-Oweini, R.; Bassil, B. S.; Friedl, J.; Kottisch, V.; Ibrahim, M.; Asano, M.; Keita, B.; Novitchi, G.; Lan, Y.; Powell, A.; Stimming, U.; Kortz, U. *Inorg. Chem.* **2014**, *53*, 5663−5673. (f) Bassil, B. S.; Ibrahim, M.; Al-Oweini, R.; Asano, M.; Wang, Z.; van Tol, J.; Dalal, N. S.; Choi, K.-Y.; Ngo Biboum, R.; Keita, B.; Nadjo, L.; Kortz, U. *Angew. Chem., Int. Ed.* **2011**, *50*, 5961−5964.

(4) Cotton, F. A.; Wilkinson, G.; Murillo, C. A.; Bochmann, M. *Advanced Inorganic Chemistry*, 3rd ed.; John Wiley & Sons, Inc.: New York, 1999; pp 830−845.

(5) (a) Sinclair, G. R.; Pilbrow, J. R.; Hutton, D. R.; Troup, G. J. *J. Magn. Reson.* **1984**, *57*, 228−238. (b) Henderson, B.; Wertz, J. E. *Defects in the Alkaline Earth Oxides*; Halstead-Wiley: New York, 1977; p 7. (c) Atsarkin, V. A.; Gerasimova, E. A.; Matveeva, I. G.; Frantsesson, A. V. *J. Exp. Theor. Phys.* **1963**, *16*, 903−904. (d) Pillbrow, J. R. *Transition Ion Electron Paramagnetic Resonance*; Clarendon Press: Oxford, U.K., 1990; Chapter 6. (e) Dalal, N. S. *In Superconductivity in Oxide Materials*; Müller, K. A., Bussmann-Holder, A., Eds.; Springer-Verlag: Berlin, 2007; Chapter 6.

(6) (a) Garanin, D. A.; Chudnovsky, E. M. *Phys. Rev. B* **1997**, *56*, 11102−11118. (b) Leuenberger, M. N.; Loss, D. *Nature* **2001**, *410*, 789−793. (c) Stamp, P. C. E.; Gaita-Arino, A. *J. Mater. Chem.* **2009**, *19*, 1718−1730.

(7) (a) Karunadasa, H. I.; Arquero, K. D.; Berben, L. A.; Long, J. R. *Inorg, Chem.* **2010**, *49*, 4738−4740. (b) Goswami, T.; Misra, A. *J. Phys. Chem. A* **2012**, *116*, 5207−5215.

(8) (a) Wassermann, K.; Lunk, H.-J.; Palm, R.; Fuchs, J. *Acta Crystallogr., Sect. C* **1994**, *50*, 348−350. (b) Wassermann, K.; Palm, R.; Lunk, H.-J.; Fuchs, J.; Steinfeldt, N.; Stoesser, R. *Inorg. Chem.* **1995**, *34*, 5029−5036. (c) Wassermann, K.; Lunk, H.-J.; Palm, R.; Fuchs, J.; Steinfeldt, N.; Stösser, R.; Pope, M. T. *Inorg. Chem.* **1996**, *35*, 3273−3279. (d) Compain, J. D.; Mialane, P.; Dolbecq, A.; Mbomekallé, I. M.; Marrot, J.; Sécheresse, F.; Duboc, C.; Rivière, E. *Inorg. Chem.* **2010**, *49*, 2851−2858. (e) Li, L.; Shen, Q.; Xue, G.; Xu, H.; Hu, H.; Feng, F.; Wang, J. *Dalton Trans.* **2008**, 5698−5700. (f) Xu, H.; Li, L.; Liu, B.; Xue, G.; Hu, H.; Fu, F.; Wang, J. *Inorg. Chem.* **2009**, *48*, 10275−10280.

(9) (a) Neese, F. *WIRES Comput. Mol. Sci.* **2012**, *2*, 73−78. (b) Neese, F. *ORCA—An ab Initio, DFT, and Semiempirical SCF-MO Package, Version 3.0.1*; Max-Planck Institute for Chemical Energy Conversion: Mülheim an der Ruhr, Germany. The binaries of ORCA are free of charge for academic users for a variety of platforms.

(10) (a) Cage, B.; Hassan, A. K.; Pardi, L.; Krzystek, J.; Brunel, L. C.; Dalal, N. S. *J. Magn. Reson.* **1997**, *124*, 495−498. (b) van Tol, J.; Brunel, L. C.; Wylde, R. J. *Rev. Sci. Instrum.* **2005**, *76*, 074101. (c) Morley, G. W.; Brunel, L. C.; van Tol, J. *Rev. Sci. Instrum.* **2008**, *79*, 064703.

(11) *SAINT*; Bruker AXS Inc.: Madison, WI, 2007.

(12) Scheldrick, G. M. *Acta Crystallogr., Sect. A* **2008**, *64*, 112−122.

(13) Malmqvist, P.-Å.; Roos, B. O. *Chem. Phys. Lett.* **1989**, *155*, 189−194.

(14) (a) Angeli, C.; Cimiraglia, R.; Malrieu, J.-P. *Chem. Phys. Lett.* **2001**, *350*, 297−305. (b) Angeli, C.; Cimiraglia, R.; Evangelisti, S.; Leininger, T.; Malrieu, J.-P. *J. Chem. Phys.* **2001**, *114*, 10252−10264. (c) Angeli, C.; Cimiraglia, R.; Malrieu, J.-P. *J. Chem. Phys.* **2002**, *117*, 9138−9153. (d) Angeli, C.; Bories, B.; Cavallini, A.; Cimiraglia, R. *J. Chem. Phys.* **2006**, *124*, 054108.

(15) Weigend, F.; Ahlrichs, R. *Phys. Chem. Chem. Phys.* **2005**, *7*, 3297−3305.

(16) (a) Perdew, J. P. *Phys. Rev. B* **1986**, *33*, 8822−8824. (b) Becke, A. D. *Phys. Rev. A* **1988**, *38*, 3098−3100. (c) Perdew, J. P. *Phys. Rev. B* **1986**, *34*, 7406.

(17) (a) Atanasov, M.; Ganyushin, D.; Sivalingam, K.; Neese, F. *Struct. Bonding (Berlin)* **2012**, *143*, 149−220. (b) Atanasov, M. A.; Zadrozny, J. M.; Long, J. R.; Neese, F. *Chem. Sci.* **2013**, *4*, 139−156. (c) Zadrozny, J. M.; Xiao, D. J.; Atanasov, M.; Long, G. J.; Grandjean, F.; Neese, F.; Long, J. R. *Nat. Chem.* **2013**, *5*, 577−581.

(18) (a) Schäffer, C. E.; Jørgensen, C. K. *Mol. Phys.* **1965**, *9*, 401−412. (b) Schönherr, T. *Top. Curr. Chem.* **1997**, *191*, 87−152. (c) Larson, E.; LaMar, G. N. *J. Chem. Educ.* **1974**, *51*, 633−640. (d) Bridgeman, A. J.; Gerloch, M. *Prog. Inorg. Chem.* **1996**, *45*, 179−281. (e) Figgis, B. N.; Hitchman, M. A. *Ligand Field Theory and Its Applications*; Wiley-VCH: New York, 2000; pp 53−60.

(19) Bi, L.-H.; Dickman, M. H.; Kortz, U.; Dix, I. *Chem. Commun.* **2005**, 3962−3964.

(20) (a) Wu, Q.; Li, Y.-G.; Wang, Y.-H.; Zhang, Z.-M.; Wang, E.-B. *Inorg. Chem. Commun.* **2010**, *13*, 66−69. (b) Zhang, D.; Zhang, Y.; Zhao, J.; Ma, P.; Wang, J.; Niu, J. *Eur. J. Inorg. Chem.* **2013**, *2013*, 1672−1680.

(21) Bi, L.-H.; Wang, B.; Hou, G.-F.; Li, B.; Wu, L.-X. *CrystEngComm* **2010**, *12*, 3511−3514.

(22) Ritchie, C.; Alley, K. G.; Boskovic, C. *Dalton Trans.* **2010**, *39*, 8872−8874.

(23) Clemente-Juan, J. M.; Coronado, E.; Forment-Aliaga, A.; Galán-Mascarós, J. R.; Giménez-Saiz, C.; Gómez-García, C. J. *Inorg. Chem.* **2004**, *43*, 2689−2694.

(24) Dong, X.; Zhang, Y.; Liu, B.; Zhen, Y.; Hu, H.; Xue, G. *Inorg. Chem.* **2012**, *51*, 2318−2324.

(25) Liu, B.; Li, L.; Zhang, Y.; Ma, Y.; Hu, H.; Xue, G. *Inorg. Chem.* **2011**, *50*, 9172−9177.

(26) Barsukova-Stuckart, M.; Izarova, N. V.; Barrett, R. A.; Wang, Z.; van Tol, J.; Kroto, H. W.; Dalal, N. S.; Jiménez-Lozano, P.; Carbó, J. J.; Poblet, J. M.; von Gernler, M. S.; Drewello, T.; de Oliveira, P.; Keita, B.; Kortz, U. *Inorg. Chem.* **2012**, *51*, 13214−13228.

(27) Veigele, W. J.; Henry, E. M. *Am. J. Phys.* **1968**, *36*, 800−802.

(28) Simulation of the experimental magnetic data was performed with the *julX* program: Bill, E. *julX*; Max-Planck Institute for Chemical Energy Conversion: Mülheim an der Ruhr, Germany.

(29) (a) Alonso, P. J.; Arauzo, A. B.; Garcia-Monforte, M. A.; Garcia-Rubio, I.; Martin, A.; Menjon, B.; Rillo, C. *Dalton Trans.* **2011**, *40*, 853−861. (b) Mohrmann, L. E.; Garrett, B. B.; Lewis, W. B. *J. Chem. Phys.* **1970**, *52*, 535−538. (c) Semenaka, V. V.; Nesterova, O. V.; Kokozay, V. N.; Dyakonenko, V. V.; Zubatyuk, R. I.; Shishkin, O. V.; Boča, R.; Jezierska, J.; Ozarowski, A. *Inorg. Chem.* **2010**, *49*, 5460−5471. (d) Carlin, R. L. *Science* **1985**, *227*, 1291−1295. (e) Abragam, A.; Bleaney, B. *Electron Paramagnetic Resonance of Transition Ions*; Oxford Press: Oxford, U.K., 1970; pp 430−433. (f) Pedersen, E.; Toftlund, H. *Inorg. Chem.* **1974**, *13*, 1603−1612. (g) Bernheim, R. A.; Reichenbecher, E. F. *J. Chem. Phys.* **1969**, *51*, 996−1001.

(h) McGarvey, B. R. *J. Chem. Phys.* **1964**, *41*, 3743−3758. (i) Bonomo, R. P.; Di Bilio, A. J.; Riggi, F. *Chem. Phys.* **1991**, *151*, 323−333.

(30) (a) Weltner, W., Jr. *Magnetic Atoms and Molecules*; Van Nostrand-Reinhold Co. Ltd.: New York, 1983; pp 42−46. (b) Chen, W.-Z.; Cotton, F. A.; Dalal, N. S.; Murillo, C. A.; Ramsey, C. M.; Ren, T.; Wang, X. *J. Am. Chem. Soc.* **2005**, *127*, 12691−12696.

(31) Weil, J. A.; Bolton, J. R. *Electron Paramagnetic Resonance Elementary Theory and Practical Applications*, 2nd ed.; Wiley-Interscience: Hoboken, NJ, 2007; pp 99−111.

(32) (a) Nellutla, S.; van Tol, J.; Dalal, N. S.; Bi, L.-H.; Kortz, U.; Keita, B.; Nadjo, L.; Khitrov, G. A.; Marshall, A. G. *Inorg. Chem.* **2005**, *44*, 9795−9806. (b) Mal, S. S.; Dickman, M. H.; Kortz, U.; Todea, A. M.; Merca, A.; Bögge, H.; Glaser, T.; Müller, A.; Nellutla, S.; Kaur, N.; van Tol, J.; Dalal, N. S.; Keita, B.; Nadjo, L. *Chem.—Eur. J.* **2008**, *14*, 1186−1195.

(33) Neese, F.; Solomon, E. I. *Magnetism: Molecules to Materials IV*; Miller, J. S., Drillon, M., Eds.; Wiley-VCH: New York, 2002; pp 345−466. Notice a sign error in eq 239 of this reference.

(34) Griffith, J. S. *The Theory of Transition-Metal Ions*; Cambridge University Press: New York, 1971; p 437, Table A.6.1.

(35) Reinen, D.; Atanasov, M.; Lee, S.-L. *Coord. Chem. Rev.* **1998**, *175*, 91−158.